Results of a Comprehensive Atmospheric Aerosol-Radiation Experiment in the Southwestern United States.*

Part II: Radiation Flux Measurements and Theoretical Interpretation

J. J. DELUISI,[1] P. M. FURUKAWA,[2] D. A. GILLETTE AND B. G. SCHUSTER[3]

*National Center for Atmospheric Research,** Boulder, Colo. 80303*

R. J. CHARLSON AND W. M. PORCH[4]

Departments of Civil Engineering, Water and Air Resources, University of Washington, Seattle 98195

R. W. FEGLEY

Mauna Loa Observatory, NOAA ARL, Hilo, Hawaii 96720

B. M. HERMAN AND R. A. RABINOFF

Department of Atmospheric Sciences, University of Arizona, Tucson 85721

J. T. TWITTY[5] AND J. A. WEINMAN

Department of Meteorology, University of Wisconsin, Madison 53706

(Manuscript received 17 November 1975)

ABSTRACT

The experimental results in Part I are used in the theoretical interpretation of the radiation flux measurements which were taken with an aircraft. The absorption term of the complex refractive index of aerosols is estimated to be approximately 0.01 for a real part of 1.5 for the wavelength bandwidth 0.32–0.68 μm. A regional variation in the refractive index is noted.

Atmospheric heating and cooling rates due to aerosol and molecular absorption in the solar and terrestrial wavelengths are determined from the radiation flux measurements. The magnitudes of these rates are compared and their relative importance is discussed.

1. Introduction

Part I of this paper described the minimum set of necessary measurements to enable theoretical analysis of the optical properties of an aerosol which determine its absorption and scattering characteristics. Part II deals with the measurement of the vertical radiative fluxes at the top and bottom of a slab of atmosphere in which the other necessary measurements have been made concurrently. The radiation flux measurements provide an estimate of the magnitude of the absorption (and, consequently, the sensible heating) of solar radiation by aerosols and molecules. The most important molecular absorber is water vapor. Oxygen absorbs in a rather narrow band at 0.76 μm, but the effect is small compared to water vapor absorption which starts near 0.70 μm and continues into the longer wavelength region beyond 3.0 μm. The effects of water vapor absorption are selectively avoided by the proper choice of spectral filters that confine measurement of radiation to a band region of the solar spectrum where absorption in a slab of atmosphere is due almost entirely to aerosols. The rate of absorption by aerosols in itself is important to the studies of dynamical meteorological phenomena and climate. For use in prediction and modeling, however, the refractive index is a more versatile parameter

* First GAARS field test.

** The National Center for Atmospheric Research is sponsored by the National Science Foundation.

[1] Present affiliation: NOAA, Air Resources Laboratories, Boulder, Colo. 80302.

[2] Present affiliation: Wright Patterson AFB, Dayton, Ohio 45433.

[3] Present affiliation: Los Alamos Scientific Laboratory, Los Alamos, N. M. 87544.

[4] Present affiliation: Lawrence Livermore Laboratory, Livermore, Calif. 94550.

[5] Present affiliation: NASA-Langley Research Center, Hampton, Va. 23665.

since it is a property of the aerosol alone, being related to the physical processes of scattering and absorption.

Our procedure for estimating a complex refractive index is to specify all necessary parameters for radiative transfer calculations with the exception of the imaginary part of the complex refractive index, which is the absorption term and which remains as the single unknown variable. Theoretical radiative transfer calculations are performed as a function of absorption refractive index, giving the variation of absorption with refractive index for a slab of atmosphere. This absorption function is then used to deduce an *effective refractive index* from the actually measured absorption occurring in a slab of atmosphere. The real part of the refractive index can be specified with reasonable accuracy; for the present investigation it is obtained from the works of other investigators.

The spectral resolution of our radiation measuring instrumentation allows us also to estimate the rate of absorption of solar radiation by water vapor, which can be compared with the aerosol absorption.

2. Radiation flux measurements

The radiation sensors used to measure the vertical hemispheric fluxes through a specified level of the atmosphere are Eppley pyranometers equipped with hemispheric Schott glass cutoff filters (see, for example, Ångström and Drummond, 1959). Three upward- and three downward-facing pyranometers permitted spectral resolution of the solar radiation into three bandwidths. The wavelength cutoffs are located at approximately 0.530 μm with the OG1 filter and 0.685 μm with the RG8 filter. WG7 quartz filters (0.27–3.3 μm) on two of the pyranometers enabled measurement of solar radiation to be made over practically the entire solar spectrum.

Table 1 summarizes the centers of the wavelength bands according to the median power of extraterrestrial solar flux as defined by the bandwidths. The extraterrestrial flux quantities are from Thekaekara (1970). Also shown in Table 1 are the extraterrestrial radiant power and the percentage of the total solar flux contained in each wavelength band. A small allowance is made for the ozone cutoff below 0.32 μm and for the longwave filter cutoff near 3.0 μm. Two Eppley infrared pyrgeometers were used to measure the terrestrial radiation in a bandwidth of 4–40 μm. A discussion of the infrared data is reserved for a separate section. The infrared and solar radiation sensors cover the important range of the electromagnetic spectrum in which there are the sources and sinks of radiant energy that heat and cool the planet and supply the power needed to drive the circulations of the oceans and atmosphere.

TABLE 1. Band centers of aircraft radiometer system.

Cutoff (μm)		Band center (μm)	Band power (cal cm^{-2} min^{-1})	Percent of solar constant*
WG7	Open	0.735	1.90	98
OG1	0.530	0.961	1.35	71
RG8	0.685	1.045	1.01	53
WG7–OG1,	$0 \rightarrow 0.530$	0.445	0.476	25
WG7–RG8,	$0 \rightarrow 0.685$	0.505	0.818	43
OG1–RG8,	$0.530 \rightarrow 0.685$	0.595	0.362	19

* Based on a solar constant of 1.942 cal cm^{-2} min^{-1}.

The sensors were mounted on pods that were bolted to the top and bottom of the aircraft fuselage. An eight channel, custom-built amplifier system raised the sensor millivolt output signal to a level compatible with the aircraft's data acquisition system. The pods and sensors were located in the airstream, which provided strong ventilation for reducing thermal gradients across the sensor: this position was selected to minimize a potential source of error. On the basis of reproducibility the precision of the entire system is estimated to be on the order of 0.5–1.0% over the dynamic range in which we were operating. The entire radiation measurement system was only marginally capable of meeting the specifications for the experiment, but it was the best that could be implemented in view of the financial constraints that existed.

Radiation data were recorded by the aircraft data acquisition system at the rate of one count per second. Instrument calibrations were applied during the processing of the data by computer. One-minute running averages of the data were used to represent a flux value near the center of the flight path which was estimated by the flight time required for a single pass over the experiment site. In most cases, more than one pass was made at nearly all levels sampled. During intervals of stable flight 1 min samples gave standard deviations on the order of 1% of the mean value. The data for each level were averaged to reduce the possibility of bias introduced by time differences and by the difficulty in maintaining a precisely horizontal attitude of the aircraft at all times. Since the attitude of the aircraft was not recorded, a certain degree of subjectivity was necessary in the analysis of the radiation data.

Whenever possible, daytime experiment flights were scheduled to span 1200 local time because zenith angle corrections are smallest then and the change of the cosine of solar zenith angle with time is also at a minimum. Nighttime flights for infrared and lidar measurements were usually started at dusk to ensure sufficient visibility during the time the lowest level was being sampled by the aircraft.

a. Solar radiation data

Table 2 is a summary of the net solar radiation data obtained by the aircraft radiometer system. Data from only two of the three Schott filters are used in the present analysis since we found it desirable to take

TABLE 2. Summary of WG7 − RG8 solar radiation measurements from aircraft.

Flight no.	Location	P (mb)	Sun zenith angle (deg)	Net*	Absorption*	Ratio**
1	Rice	980	13.8	0.601	0.016	0.020
		580		0.617		
5	Quartzite	980	19.8	0.595	0.033	0.043
		540		0.628		
7	Quartzite	980	20.3	0.570	0.039	0.053
		580		0.609		
8	Big Spring	920	12.0	0.667	0.021	0.027
		660		0.688		
9	Big Spring	920	44.2	0.453	0.013	0.025
		660		0.466		
11	Big Spring	920	39.6	0.491	0.019	0.033
		660		0.510		

* Units cal cm^{-2} min^{-1}.
** Absorbed flux to incident flux.

advantage of the larger signal-to-noise ratio. The wavelength regions determined by the WG7 and RG8 filters gave the most reliable results.

The solar zenith angle at the time of the aircraft's lowest altitude was selected as the reference for each set of data. Because of the time change of solar zenith angle, data taken at the higher altitudes were adjusted to conform with the reference zenith angle. This was accomplished by using functions of theoretical estimates of the change in flux with solar zenith angle. For example, if a measurement period began when the solar zenith angle was 20° and ended when it was 15°, then the fractional change in the theoretical estimate from 20° to 15° was used to adjust the real data back to a 20° solar zenith angle. In effect, this procedure eliminated the need to include a direct time-rate-of-change relationship in the theoretical interpretation of the data. We have not made a thorough study of the possible errors associated with the zenith angle corrections. We do feel, however, that the errors are no worse than the errors due to inhomogeneities in surface reflectivity and to variations in aerosol concentrations that occur in space and time.

During Flights 7 and 8, the WG7 downward-facing pyranometer failed to function properly at some levels. When needed, estimates were made of the upwelling fluxes in the WG7 band on the basis of the other data.

The data shown in the last two columns of Table 2 give the absorption of solar radiation in the WG7–RG8 band. The absorption rate is given in calories per square centimeter per minute (1 cal cm^{-2} min^{-1} = 697.7 W m^{-2}). The last column represents the fractional absorption of radiation with respect to the incoming total radiation measured at the highest level flown by the aircraft. The ratio multiplied by 100 gives the percentage of incident radiation absorbed by the slab of atmosphere being sampled. If we take into account the different optical depths of aerosols (see τ_d in Table 5), we note that the average absorption is greater at Blythe than at Big Spring: this difference is discussed in the section on refractive index.

With radiation measurements there is always the danger of encountering systematic error because of uncertainties in calibration. In our case, using the sun as a source, the spectral variation of radiation intensity is still not adequately resolved, according to recent reports and meetings on the subject. By taking the ratio of absorption to incident flux, the reliance on absolute measurements is virtually eliminated and error effects due to possible systematic differences between the individual sensors are greatly diminished.

b. Heating of the atmosphere by aerosols

Measurement of the rate of absorption by aerosols permits an estimate of the heating taking place. Table 3, under the column heading Total aerosol absorption, presents estimates of the absorption from 0.3 to 3.0 μm. The aerosol absorption in the RG8 band has been estimated by multiplying the WG7–RG8 band absorption by a factor of 0.923, which has been derived from the ratio of solar power in the RG8 band to the WG7–RG8 band and from the change in aerosol optical depth. It is assumed that the aerosol absorption rate is not highly dependent on wavelength, an assumption that is justified from the findings of Kondratyev *et al.*

TABLE 3. Comparison of aerosol absorption with molecular absorption.

Flight no.	Location	Absorption WG7	Absorption WG7–RG8	Estimate RG8 for aerosol*	Total aerosol absorption	Gas absorption	Percent aerosol to gas
1	Rice	0.147	0.016	0.016	0.032	0.115	28
5	Quartzite	0.200	0.033	0.032	0.065	0.135	48
7	Quartzite	0.153	0.039	0.038	0.077	0.076	101
8	Big Spring	0.162	0.021	0.020	0.041	0.121	34
9	Big Spring	0.089	0.013	0.013	0.026	0.063	41
11	Big Spring	0.119	0.019	0.018	0.037	0.082	45
						Average	50

* Estimate = 0.923(WG7 − RG8 absorption).

(1974). Total absorption by aerosols is found by adding the absorption in the WG7–RG8 band and the estimated absorption in the RG8 band. The absorption by water vapor and other gases in the RG8 band is estimated by subtracting the total absorption by aersols from the absorption over the entire solar spectrum in the WG7 band.

The last column of Table 3 gives the percent absorption of aerosol to gas, and the final figure gives the average. Although the value for Flight 7 departs quite markedly from the other values, it is nevertheless included in the average.

From the first law of thermodynamics a simple formula giving heating as a function of absorption rate and pressure differences between the upper and lower boundaries of a slab is

$$\frac{dT}{dt} = 288.2 \frac{F_a(\Delta P)}{\Delta P}, \tag{1}$$

where dT/dt is the rate of change of temperature with time (K h^{-1}) and $F_a(\Delta P)$ is the flux absorption in a layer of thickness ΔP (mb). According to the data in Table 3, the average heating by aerosols is 0.039 K h^{-1} in an atmosphere with average thickness of 337 mb. This rate also depends on the solar zenith angle. The total absorption due to aerosols and water vapor is given by the WG7 data under the column heading Absorption WG7. The average heating of the atmosphere for this absorption rate is 0.12 K h^{-1}, which is approximately three times greater than by aerosols alone. These results are not unlike results reported by Kondratyev *et al.* (1974), and by Dummond and Robinson (1974). The average vertical distribution of heating by aerosols should follow roughly the average vertical distribution of aerosols shown in Fig. 8, Part I. Although the aircraft measurements were made at four to six levels in the atmosphere, the solar radiation data have been analyzed completely only for the top and bottom levels because these are the only measurement levels needed for the determination of the refractive index of the aerosols. No attempt has been made to determine the absorption by aerosols as a function of altitude.

TABLE 4. Atmospheric water vapor and pressure correction: W is precipitable water and P pressure.

Flight no.	W (cm)	P/P_0	$(P/P_0)^{0.75}$	$W(P/P_0)^{0.75}$
1	0.92	750/980	0.82	0.75
5	1.03	720/980	0.79	0.81
7	0.80	880/980	0.92	0.74
8	0.89	810/900	0.92	0.83
9	0.19	820/900	0.93	0.18
11	0.71	780/900	0.90	0.64
Average	0.76			0.66

Table 4 shows total water vapor amounts (cm) in the slabs of atmosphere flown by the aircraft. These data were obtained from the nearest radiosonde stations for times corresponding most closely to the times of the experiments. A very low water vapor amount is seen for Flight 9, and a low aerosol optical depth had been observed (see Fig. 4, Part I). Also, the data in Table 3 showing absorption by the important gases seem to correlate reasonably well with the total amount of water vapor (some radiosonde stations were greater than 70 km from the experiment sites).

In Table 4 we have applied crude pressure corrections to the water vapor amounts. The exponent of the pressure correction is somewhat arbitrary, having a range from 0.5 to 1.0, according to Lacias and Hansen (1974). Using the corrected water vapor values and allowing for about 6% more for the water vapor in the atmosphere above the highest levels flown by the aircraft and using the absorptivities given by Yamamoto (1962), we estimated an average absorption of about 0.09 cal cm^{-2} min^{-1} for a surface reflectivity of zero. This compares quite well with the average gas absorption of 0.099 cal cm^{-2} min^{-1} shown in Table 3. Indeed, the result increases our confidence in the simple procedure we followed for estimating aerosol absorption in the RG8 band. If the reflectivity of the surface were included in the calculation, the absorption by water vapor would be higher, and likely would provide better agreement with observation.

c. *Surface reflectivity*

The reflectivity of the surface is easily measured by the instrumentation aboard the aircraft. For the lowest altitude flown by the aircraft (20–40 m), the ratio of the upwelling to downwelling radiation gives the reflectivity data needed for the solution for the refractive index of aerosols. Fig. 1 shows the average reflectivity for surfaces at Rice, Calif., Quartzite, Ariz., and Big Spring, Tex. Spectral resolution is obtained by subtracting the radiation measurements in the different filter bands. Data for the spectral bands are labeled as WG7–OG1, etc., while data for the individual filters are labeled WG7, OG1, etc. The reflectivities for the bands are connected by straight lines.

A very interesting feature of Fig. 1 is that the surface reflectivity of the WG7–OG1 band is nearly the same at all sites. A sharp separation occurs at the OG1–RG8 band, in which the desert soil reflects three times as strongly as the soil at Big Spring, where the soil is darker and there is more vegetation. All sites showed an increase in surface reflectivity in the RG8 band, or the red region, of the solar spectrum. Although the reflectivity data in the WG7–RG8 band that are used for the analysis of refractive index are not shown in Fig. 1, they are given for each measurement episode in Table 5.

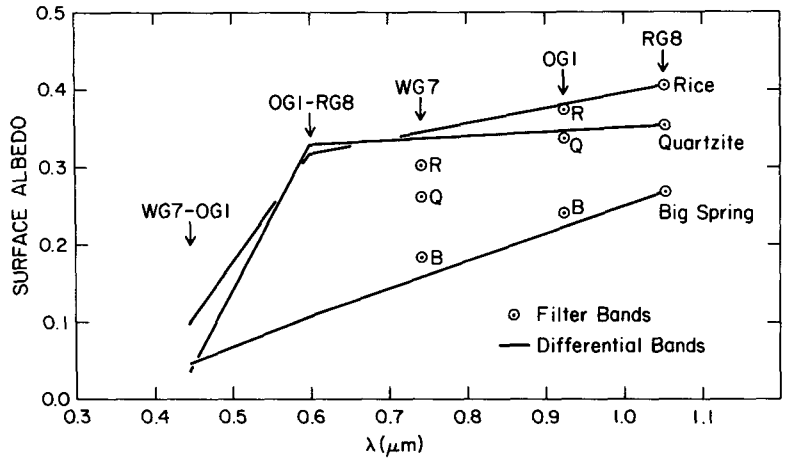

FIG. 1. Surface albedo as a function of wavelength. Straight lines connect the values of surface albedo for the differential bands (e.g., OG1–RG8), and circles with dots represent surface albedo for the entire band (e.g., WG7). R, Q and B stand for Rice, Quartzite, and Blythe.

3. Aerosol refractive index

The refractive index of a material is expressed conventionally as a complex number $n_1 - in_2$. The real part is related to the velocity of propagation and the imaginary part to the decay of electromagnetic energy in a medium with certain dielectric, magnetic permeability and conductivity properties. Atmospheric aerosols are generally inhomogeneous in composition and size, although the size distribution of particles falls off rather rapidly above a particle radius of 10 μm because of the shorter atmospheric residence times of the larger particles. In principle, the optical properties of each aerosol particle can be measured and a net radiative effect can then be inferred by summing the individual effects over a large volume of atmosphere. The difficulty of such an approach is immediately apparent in that the solution to the problem is not only highly formidable but also impractical because of the resources that would be required to carry through a meaningful program of research.

Therefore, our approach is via the observations of macroscopic phenomena, from which we deduce and ascribe single variables and simplified functions that are representative of the average behavior of an idealized but naturally inhomogeneous atmosphere. This approach is most meaningful in its application to large-scale major problems of effects on the earth's energy exchange processes.

Fig. 2 shows solutions of theoretical radiative transfer calculations for a vertically inhomogeneous, plane-parallel atmosphere containing aerosols and molecules (Herman and Browning, 1965: Herman *et al.*, 1975). The solutions for an optical depth τ_d are in terms of the ratio of radiant flux absorbed to incident flux at the top of the atmosphere as functions of the imaginary term n_2 of the complex refractive index, the solar zenith angle θ_0, and the surface reflectivity A. The aerosol size distribution for these calculations are of the Junge (1957) form, with a slope of -2 which approximates, but does not cover, the range of variation of the observed size distributions shown in Part I.

TABLE 5. Summary of refractive indices.

Flight no.	Location	A	τ_d	θ_0	R	ϵ	n_2	$n_2+\delta_1$	$n_2-\delta_2$
1	Rice	0.203	0.056	13.8	0.020	1.04	0.016	>0.1	0.0
5	Quartzite	0.152	0.150	19.8	0.043	0.51	0.011	0.024	0.006
7	Quartzite	0.169	0.117	20.3	0.053	0.40	0.014	0.032	0.008
8	Big Spring	0.103	0.089	12.0	0.027	0.80	0.009	0.035	0.003
9	Big Spring	0.077	0.082	44.2	0.025	0.85	0.010	0.070	0.001
11	Big Spring	0.066	0.136	39.6	0.033	0.64	0.008	0.019	0.002

Mean (1, 5, 7) = 0.014 (0.052, 0.005)*
Mean (8, 9, 11) = 0.009 (0.024, 0.002)*

* Upper and lower bound due to δ_1 and δ_2.

A surface reflectivity
τ_d aerosol optical depth
θ_0 sun zenith angle
R ratio of absorbed to incident flux
ϵ error estimate (cal cm^{-2} s^{-1})
n_2 solution refractive index
δ error increment (see text).

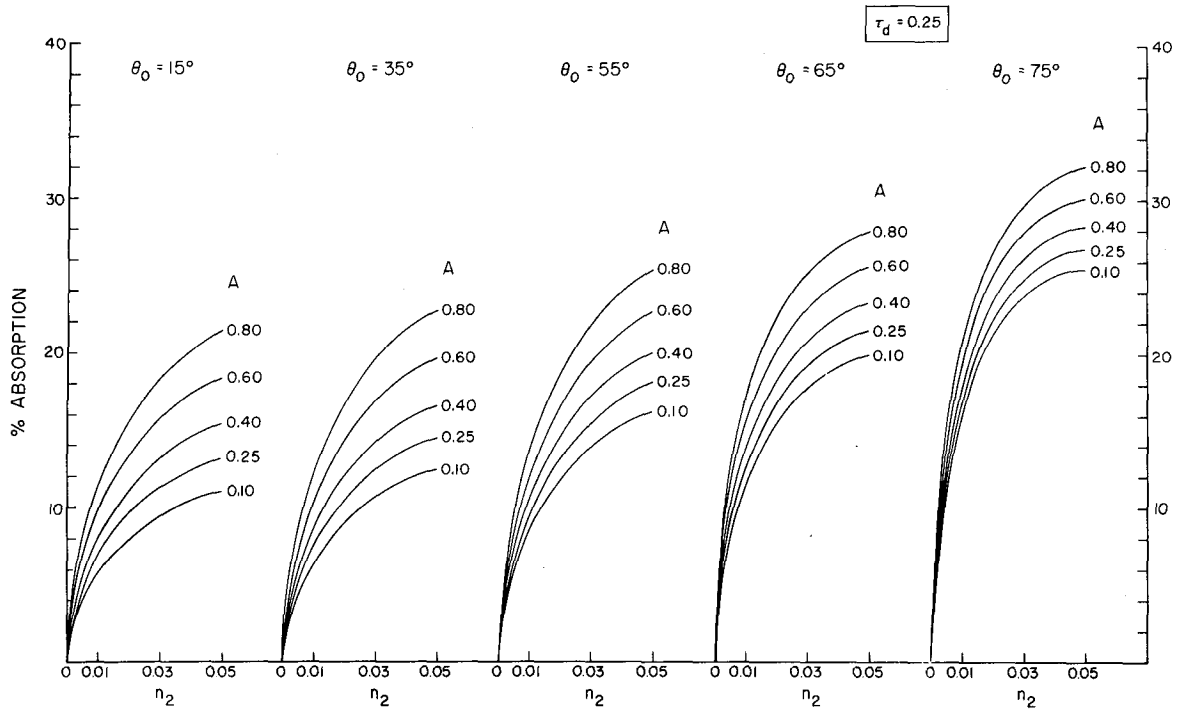

FIG. 2. Theoretically calculated functions of the percent of absorption of solar power to the incident power as a function of the imaginary term of the refractive index of aerosols having a Junge size distribution form and a slope of -2. The solar zenith angle is given by θ_0, τ_d is the optical depth of dust, and A is the albedo of the surface. A standard atmosphere with surface pressure of 1000 mb is used in theoretical calculation.

The real term of the complex refractive index has been preselected as 1.5 on the basis of existing information on desert aerosols (Pollack *et al.*, 1973; Grams *et al.*, 1974; Herman *et al.*, 1975).

With all of the necessary variables prespecified by the measurements from Part I, functions of the type shown in Fig. 2 were used to deduce an imaginary term of the refractive index on the abscissa. Interpolations were performed for values lying between the functions representing discrete values of the variables shown in Fig. 2. Another set of functions similar to Fig. 2 was calculated for $\tau_d = 0.10$. Table 5 summarizes the results of the field observations which provided all of the variables needed to deduce the imaginary refractive indices. The third column from the last is the solution refractive index and the last two columns are the solutions for $\pm 1\%$ error (i.e., $\pm\delta$) in the radiation observations for the upward viewing pyranometer, specifically with the WG7 filter which gives the highest power reading of any of the solar radiation measuring instruments on the aircraft. The 1% error has a very large effect on the magnitude of the absorption refractive index. The problem of error becomes worse for weakly absorbing aerosols. The fractional change of the absorption due to the estimated error is shown as ϵ in Table 3. The magnitude of the error is on the pessimistic side; this choice was made deliberately to override other significant sources of uncertainty in the observations of the independent variables. Specific radiative transfer calculations for the refractive index for each episode would be ideal, but because of the uncertainties in the prespecified variables it would be difficult to justify the rather large amount of computer time that would be needed.

From the care that was exercised in the development of the pyranometer instrumentation system, a more realistic estimate of uncertainty of the measurements would be on the order of 0.5%, which is nearly in line with the characteristics of a similar measurement system used by Drummond and Robinson (1974). We should point out that our method of analysis finds an absorption by virtue of a difference in observed radiation quantities; as a result, the relative response of the instrument is most important.

Table 5 also summarizes the mean values of absorption refractive index for the Blythe (Flights 1, 5 and 7) and Big Spring (Flights 8, 9 and 11) areas. Estimates of the average uncertainty are given with each refractive index. The uneven spread between the high and low ranges of the uncertainties are due to the nonlinear dependence of radiation absorption by aerosols suspended in the atmosphere (see Fig. 2).

We do not have a concrete explanation for the 50% difference in the deduced absorption refractive indices for the Blythe and Big Spring areas. Since no chemical composition measurements were made, it is not possible

for the different refractive indices to be directly attributed to a possible difference in chemistry. We can, however, on the basis of the CAENEX (Complex Atmospheric Energetics Experiment) results reported by Kondratyev *et al.* (1974), speculate that the desert aerosols might contain higher concentrations of radiation-absorbing iron compounds than the aerosols over the agricultural region of Big Spring.

We have considered the effect of the darker albedo of the surrounding hills in the vicinity of the Blythe experiment sites which could bias the measurement of the upwelling radiation when the aircraft was sampling the higher altitudes. As the altitude of the aircraft increases, greater portions of the nearby hills are included in the 2π angle of view of the downward-facing instruments. However, we believe the effect is rather small, having no serious consequence on the final results.

We are unaware of any results from other investigations that can be usefully compared on an equivalent basis with our results. From measurements of the scattering phase function Grams *et al.* (1974) deduced a value $n_2=0.005$ for airborne soil particles near the surface at Big Spring. Refractive indices of terrestrial rocks and glasses (Pollack *et al.*, 1973), which could conceivably be a part of the local aerosol, are an order of magnitude smaller than the results in Table 5.

Lindberg and Laude (1974) reported values of n_2, including the variation with wavelength, for atmospheric aerosols collected 3 m above the surface in southwestern New Mexico. Their laboratory analysis, based on the Kubelka-Munk theory, showed an increase of n_2 with decreasing wavelength in the near-UV region. According to their results, the New Mexico aerosols have an effective n_2 ranging from 0.008 to 0.011 (rather close to the results in Table 5) over the WG7–RG8 bandwidth, weighted according to the spectral variation of the incident solar flux. For industrialized areas, Eiden (1966) deduced values of n_2 ranging from 0.1 to 0.01 from polarization data at Mainz, and Lin *et al.* (1973), using the opal glass technique, deduced values of n_2 ranging from 0.03 to 0.05 for New York City air, where the wavelength of radiation is near the maximum power output of the solar spectrum. The magnitude of refractive indices for aerosols in industrial areas is quite large compared to those for aerosols derived from natural sources.

We find that n_2 values fall in the range of n_2 values resulting from the CAENEX program, i.e., $0.005 \leqslant n_2 \leqslant 0.015$ (Kondratyev, 1974). The refractive index of aerosols has been observed to vary significantly at locations not greatly separated in distance. Although these variations were not unexpected, and granting that methods for determining refractive indices differ, from what little supporting evidence that exists the picture that is beginning to emerge is that aerosol optical properties are quite variable in space (and also quite likely in time). These findings imply that if the radiative effects of aerosols are ever to be included in *realistic*, three-dimensional global models depicting the energy exchange processes that control weather and climate, it will be necessary to account for the variable optical properties of aerosols.

It is possible to analyze our field data for the imaginary term of the refractive index using the diffuse-direct method recently reported by Herman *et al.* (1975). This method appears to be potentially superior to the absorption method. The necessary variables are the hemispheric fluxes, aerosol optical depth and surface reflectivity. The downward total flux measured by the aircraft pyranometer system can be separated by estimating the direct radiation with the use of Beer's law, given the optical depth of aerosols and Rayleigh scattering (see Part I). The wide bandwidth of the WG7–RG8 filters can introduce some serious uncertainties when Beer's law is used.

For the present analysis, we consider only average values, because of measurement uncertainties in the data, and because the data are not specific to the diffuse-direct method. From Tables 1 and 2 in Part II, and using the optical depth data from Part I, we arrive at the following average values for the three desert experiment episodes which were chosen because of small differences in the solar zenith angle:

Downward direct and diffuse flux near surface for (WG7–RG8)	0.714 cal cm^{-2} min^{-1}
Extraterrestrial solar flux (see Table 1)	0.818 cal cm^{-2} min^{-1}
Optical depth of aerosol from surface to top of the atmosphere	0.122 atm^{-1}
Surface pressure	960 mb
Rayleigh optical depth (5000 Å)	0.137 atm^{-1}
Solar zenith angle	24.5°
Ozone absorption (estimated from Lacias and Hansen, 1974)	0.12 cal cm^{-2} min^{-1}
Surface reflectivity	0.17
Diffuse-direct ratio	0.218
Solution refractive index from Herman *et al.* (1975)	0.008

In view of the large uncertainties in the technique we used to obtain the diffuse radiation, our solution $n_2=0.008$ is quite reasonable. This solution is closer to the Big Spring results; however, we are inclined to believe that this result is coincidental. Other uncertainties are differences between the aerosol vertical distribution and size distribution models used by Herman *et al.* (1975) and the distributions existing at the time of the field experiment.

4. Terrestrial infrared observations

The wavelength range of sensitivity of the Eppley pyrgeometers is approximately 4–40 μm. These instruments are normally calibrated against the output of a blackbody having a radiant output proportional to the fourth power of temperature. An evaluation of these instruments for use on an aircraft platform was reported by Albrecht *et al.* (1973).

Our use of infrared (IR) observations was limited to examining the behavior of the flux divergence. This

information provides us with the magnitude of IR cooling, which then can be compared with the heating by aerosols and gases.

Figs. 3 and 4 shows plots of straight lines joining the points where net fluxes were measured at the levels flown by the aircraft. Data are shown for all flights except number 4, which was terminated because of cirrus development. Negative slope indicates radiative convergence or heating and positive slope indicates radiative divergence or cooling.

For the daytime flights, a very pronounced heating appeared to occur, namely during Flights 1, 5 and 7. Flights 7 and 6 have the same net flux up to 2 km. However, although designated as a nighttime flight, Flight 6 began at an earlier time than the other two night flights to ensure sufficient daylight for the lower altitude flown. Thus, for Flight 6 and possibly others, surface temperature, affecting predominantly the upwelling flux, probably changed significantly during the time required for the ascent of the aircraft.

The IR heating that took place during Flight 1 from the surface to near 2 km was 0.068 cal cm^{-2} min^{-1}, which is about twice that for aerosols alone for the entire slab! This corresponds to a heating rate of about 0.09 K h^{-1}. Up to the highest altitude flown, total IR cooling reduced the net heating to about 0.018 cal cm^{-2} min^{-1}, which is less than half of the heating by aerosols alone over the entire solar spectrum.

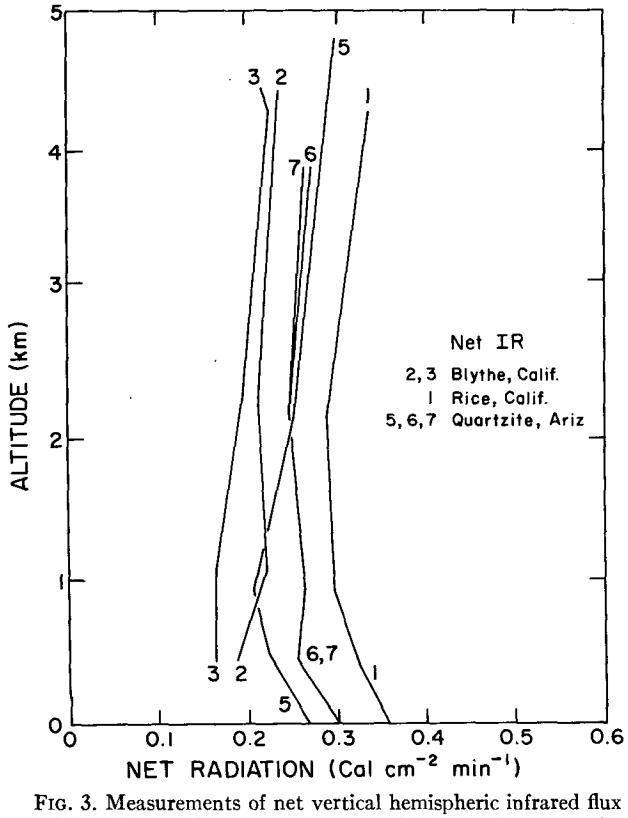

FIG. 3. Measurements of net vertical hemispheric infrared flux at Blythe, Rice and Quartzite for a bandwidth of 4–40 μm. The curves are lines connecting points at each level where a measurement was made. A flight number is given on each plot.

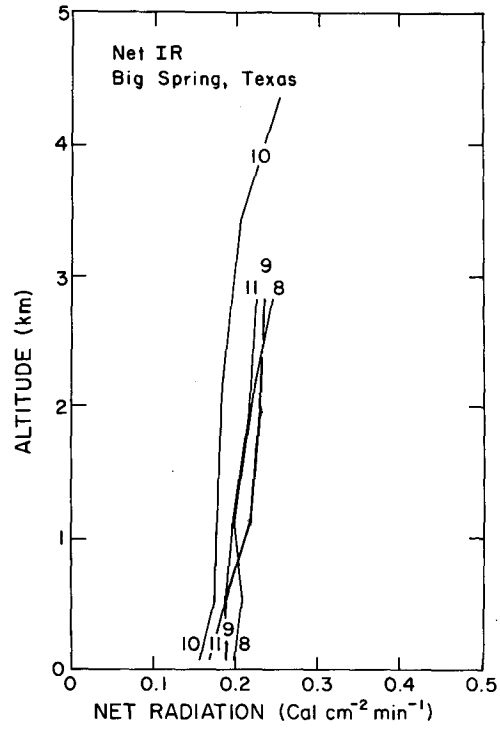

FIG. 4. As in Fig. 3 except for Big Spring.

In contrast to the daytime heating, the nighttime Flight 2 showed a net IR cooling of the entire slab of ~ -0.059 cal cm^{-2} min^{-1}, which is about equal to the rate of absorption of solar radiation by aerosols alone over the entire solar spectrum (see Table 3).

In general, the magnitude of the absorption rate of solar radiation by aerosols in the desert is about equal to the terrestrial IR cooling at night in the atmospheric slabs that we investigated. The agricultural region at Big Spring did not show terrestrial IR heating as significant as had been observed in the desert.

We have not been able to perform a detailed analysis of the part played by atmospheric aerosols in the IR, mainly because our data are inadequate. Accurate water vapor concentration data and spectral radiation measurements are required. On the other hand, model calculations of infrared radiation fluxes by Herman (1972) for the 10 μm window region indicate that effects of silicaceous aerosol can be significant; thus it would not be unreasonable to speculate that aerosols are enhancing the IR convergence and reducing cooling rates in the lowest layers of the desert atmosphere.

5. Conclusion

The first GAARS field experiment has produced plausible results. These results demonstrate the feasibility of collecting a set of measurements that would

be required to construct a physical-numerical representation (see Part I for details) of aerosol characteristics necessary for a moderately detailed understanding of their radiative behavior in the atmosphere. Aerosol size distributions, vertical distributions, and the imaginary part of their complex refractive indices have been determined in a way consistent with radiative transfer theory and with direct observations of absorption in a volume of atmosphere. The deduced refractive indices of ~ 0.01 compare favorably with the results of other investigators.

The feasibility of using remote sensing methods to determine aerosol vertical distribution by lidar and size distribution by solar aureole measurements has been demonstrated. The absorption of solar infrared $>0.7\ \mu$m by H_2O, O_2 and CO_2 was examined in a cursory manner and was found to be consistent with predictions by theoretical means. In the rather arid southwest, aerosols were found to be absorbing solar radiation (over nearly the entire solar spectrum) at a rate of about one-half the absorption by water vapor.

Infrared cooling in the terrestrial wavelength region seems to be inhibited by strong radiative convergence in the lowest few kilometers of the desert atmosphere. In a slab of atmosphere from the surface up to 4–5 km, the nighttime terrestrial infrared cooling rate is about equal to the daytime solar heating by aerosol absorption.

Limitations in time and resources did not allow us to undertake a thorough investigation that would adequately cover all important regions of the solar and terrestrial electromagnetic spectrum. The methodolgy that was adopted for the analysis and interpretation of the radiation data in the solar wavelengths appears to be suitable for future research efforts.

It is not clear yet what methods will be suitable for aerosol research in the terrestrial infrared wavelength region. Future basic research efforts should be directed more strongly at solving this important problem, for it is in the terrestrial infrared that the energy dissipative processes in the earth-atmosphere system are at work.

At the present, there are no definite plans for continuing the next and more advanced phase of the research that was originally recommended by the authors in the initial stages of the GAARS. There remains a need to study the optical behavior of a turbid atmosphere (including clouds) at different seasons and locations on the globe in order to uncover the differences and subtleties that undoubtedly exist, especially where man-made pollution is present. The Soviet Union's CAENEX is actively involved with this research problem but, to attack such a problem on the global scale, a much larger coordinated research force will be required than that which now exists.

Acknowledgments. In addition to the acknowledgments mentioned in Part I, we wish to express our sincerest thanks to W. W. Kellogg for his enthusiastic support of the GAARS concept. Appreciation is expressed to K. Hanson and S. Cox for the loan of radiation instrumentation.

Partial support for this phase of the GAARS was provided by the National Aeronautics and Space Administrations under Grants NASA-50-002-140, NSG-5046 and NGR03-002-155; by the Office of Naval Research under Contract N00014-67-A-0209-0021; and by the Atmospheric Sciences Section, National Science Foundation under Grants GA27662 and GA31562.

REFERENCES

Albrecht, B., M. Poellot and S. K. Cox, 1973: Pyrgeometer measurements from aircraft. *Rev. Sci. Instr.*, **45**, 33–38.

Ångström, A. K., and A. J. Drummond, 1959: Transmission of "cut-off" glass filters employed in solar radiation research. *J. Opt. Soc. Amer.*, **49**, 1096–1099.

Drummond, A. J., and G. D. Robinson, 1974: Some measurements of the attenuation of solar radiation during BOMEX. *Appl. Opt.*, **13**, 487–492.

Eiden, R., 1966: The elliptical polarization of light scattered by a volume of atmospheric air. *Appl. Opt.*, **5**, 569–575.

Grams, G. W., I. H. Blifford, D. A. Gillette and P. R. Russell, 1974: Complex index of refraction of airborne particles. *J. Atmos. Sci.*, **13**, 459–477.

Herman, B. M., 1972: The influence of atmospheric aerosols on the flux of infrared radiation through the atmosphere. *Preprints Conf. on Atmospheric Radiation*, Fort Collins, Colo., Amer. Meteor. Soc., 29–30.

——, and R. S. Browning, 1965: A numerical solution to the equation of radiative transfer. *J. Atmos. Sci.*, **22**, 559–566.

——, —— and J. J. DeLuisi, 1975: Determination of the effective imaginary term of the complex refractive index of atmospheric dust by remote sensing: The diffuse-direct radiation method. *J. Atmos. Sci.*, **32**, 918–925.

Junge, C. E., 1957: Air chemistry and radioactivity. *Advances in Geophysics*, Vol. 4, Academic Press, 1–108.

Kondratyev, K. Ya., O. B. Vassilyev, V. W. Grishechkin and L. S. Ivlev, 1974: Spectral radiative flux divergence and its variability in the troposphere in the 0.4–2.4 μ region. *Appl. Opt.*, **13**, 478–486.

Lacis, A. A., and J. E. Hansen, 1974: A parameterization for absorption of radiation in the earth's atmosphere. *J. Atmos. Sci.*, **31**, 118–133.

Lin, C. I., M. Baker and R. J. Charlson, 1973: Absorption coefficient of atmospheric aerosol: A method for measurement. *Appl. Opt.*, **12**, 1356–1363.

Lindberg, J. D., and L. S. Laude, 1974: Measurement of the absorption coefficient of atmospheric dust. *Appl. Opt.*, **13**, 1923–1927.

Pollack, James B., O. B. Toon and B. N. Khare, 1973: Optical properties of some terrestrial rocks and glasses. *Icarus*, **19**, 372–389.

Thekaekara, M. P., 1970: The solar constant and the solar spectrum measured from a research aircraft. NASA Rep. TR-R-351, 85 pp.

Yamamoto, G., 1962: Direct absorption of solar radiation by atmospheric water vapor, carbon dioxide and molecular oxygen. *J. Atmos. Sci.*, **19**, 182–188.